Electronic Supplementary Material (ESI) for Green Chemistry.

Supplementary Information

Microwave-assisted Low Temperature Biomass Pyrolysis: From Mechanistic Insights to Pilot Scale

Hu Luo,‡[a] Yanfei Zhang,‡[ab] He Zhu,[a] Xinpeng Zhao,[ab] Lijun Zhu,[ab] Wang Liu,[ab] Mengya Sun, [ab] Gai Miao,[a] Shenggang Li,*[abc] and Lingzhao Kong*[ab]

[a] CAS Key Laboratory of Low-Carbon Conversion Science and Engineering, Shanghai Advanced Research Institute, Chinese Academy of Sciences, Shanghai 201210, PR China.

[b] University of Chinese Academy of Sciences, Beijing 100049, PR China.

[c] School of Physical Science and Technology, Shanghai-Tech University, Shanghai 200031, PR China.

‡ These two authors contribute equally.

* Corresponding authors:

Shenggang Li, E-mail: lisg@sari.ac.cn, Lingzhao Kong, E-mail: konglz@sari.ac.cn

Address: No.99 Haike Road, Zhangjiang Hi-Tech Park, Pudong Shanghai, PR China.

Table S1. Main compounds identified in liquid products

Number	Residence time (min)	Compounds	GCMS/(area)%		
			250/^{o}C	285/^{o}C	300/^{o}C
1	2.351	Formic acid	1.77%	1.75%	1.13%
2	2.658	2,3-Butanedione	3.04%	3.01%	4.60%
3	3.301	Acetic acid	22.76%	22.51%	22.19%
4	3.474	2-Propanone, 1-hydroxy-	16.06%	15.89%	14.51%
5	5.187	1-Hydroxy-2-butanone	4.32%	4.27%	4.73%
6	5.404	Propanoic acid, 2-oxo-, methyl ester	1.14%	2.21%	0.49%
7	6.522	Furfural	6.76%	6.69%	6.43%
8	7.583	2-Furanmethanol	6.57%	6.50%	8.26%
9	7.714	1,2-Ethanediol, diacetate	2.53%	2.50%	2.52%
10	9.146	Butyrolactone	1.86%	1.84%	2.48%
11	9.289	2(5H)-Furanone	1.81%	1.79%	1.13%
12	9.619	1,2-Cyclopentanedione	2.26%	2.24%	3.28%
13	11.314	Phenol	2.34%	2.31%	1.52%
14	11.802	Oxazolidine, 2,2-diethyl-3-methyl-	2.23%	2.21%	0.58%
15	12.745	2-Cyclopenten-1-one, 2-hydroxy-3-methyl-	3.75%	3.71%	3.92%
16	14.392	P-Cresol	3.85%	3.81%	3.79%
17	14.734	Phenol, 2-methoxy-	8.76%	8.67%	10.79%
18	18.539	Benzofuran, 2,3-dihydro-	2.11%	2.09%	2.17%
19	21.229	2-Methoxy-4-vinylphenol	2.35%	2.33%	2.31%
20	22.228	Phenol, 2,6-dimethoxy-	1.88%	1.86%	2.75%

Table S2. Comparison of rice straw pyrolysis with literature reports

Material	T (°C)	Reactor	Heating rate (°C/min)	Products yields (%)			Heating method
				Solid	Liquid	Gas	
Rice straw	300-500	Fixed bed	10-12	41-57	30-38	12-20	CH [1]
Rice straw	300-450	Fixed bed	20	33.2-39.2	29.2-29.8	31.6-37.0	CH [2]
Rice straw	414-491	fluidized bed	——	19-41	41-63	18-19	CH [3]
Rice straw	500	Fixed bed	——	47.7	31.3	11.5	CH [4]
Rice straw	450-550	Fixed bed	1000	37-51	37-47	10-13	CH [5]
Rice straw	400-700	Free-fall	1000	18-36	39-46	24-49	CH [6]
Rice straw	300-450	Fixed bed	20	33-36	25-28	36-40	CH [7]
Rice straw	150-360	Fixed bed	10-50	35-55	36-46	10-20	MH [8]
Rice straw	400	Fixed bed	——	62.9	15.3	21.8	MH [9]
Rice straw	250-300	Fixed bed	20-40	35-45	33-38	17-31	this study

Table S3. Comparison of microwave-assisted pyrolysis with conventional pyrolysis

Heating method	T/ ^{o}C	Acids (area%)	Furans (area%)	Esters (area%)	Ketones (area%)	Phenols (area%)	H_2 (vol.%)	CO (vol.%)	CH_4(vol.%)	CO_2(vol.%)	
MH	250-300	22.76	5.9	1.14	11.75	30.14	8.6	39.1	4.8	47.5	
CH	400-500	19.2[a]	5.5 [a]	3.2 [a]	14.5 [a]	28.4 [a]	9.0 [b]	33.6 [b]	4.2 [b]	50.0 [b]	
Heating method	T/ oC	Gas (wt.%)	Liquid (wt.%)	Solid (wt.%)	C (wt.%)	H (wt.%)	N (wt.%)	S (wt.%)	HHV(MJ/kg)	TGA(residual)	pH
MH	250-300	17.9	36.4	45.7	47.51	3.04	0.92	0.02	15.9	32	3.2
CH	400-500	11.5 [c]	31.3 [c]	47.7 [c]	45 [c]	2.5 [c]	1 [c]	0.01 [c]	16.5 [c]	31	3.5 [d]

MH: microwave heating, CH: conventional heating.

a. D.Y. Chen et al., Fuel, 2019, 252, 1–9. *b. J.Park* et al., *Bioresource Technology, 2014, 155, 63–70*. *c. H.Nam et al., Energy, 2015, 93, 2384-2394. d. A.M. Shoaib et al., Egyptian Journal of Petroleum, 2018, 27, 1305–1311*).

Table S4. Kinetic parameters for rice straw measured in MAP and compared with CP

Biomass	Heating method	HR (K/min)	Method	*E*(kJ/mol)	*A*(1/s)
Rice Straw	CP[10]	15	Approximate integral	70-83	7.3×10^{6}-6.2×10^{13}
	CP[11]	5-15	KAS	193.6	6.9×10^{15}
	CP[12]	5-40	KAS	142-170	——
	CP[13]	10-40	DAEM	203-218	——
	CP[14]	10-100	Kissinger	66.16	9.9×10^{2}
	CP[15]	10-40	nth-order	71-106	3.1×10^{4}-9.8×10^{7}
	CP[16]	5-15	Friedman	145.52	3.7×10^{11}
	MH[14]	10-100	Kissinger	21.37	2.5×10^{-1}
	MH[8]	10-50	Isoconversional	29.88	1.6
	This study	20-40	KAS	38.87	6.3×10^{3}

Table S5. The most common kinetic models used in the isoconversion methods.

Models		Code	$f(\alpha)$	$g(\alpha)$*
Order-based	First-order	L1	$1-\alpha$	$-\ln(1-\alpha)$
	Second-order	L2	$(1-\alpha)^2$	$(1-\alpha)^{-1}-1$
	Third-order	L3	$(1-\alpha)^3$	$[(1-\alpha)^{-2}-1]/2$
Diffusional	1-D diffusion	D1	$1/2\alpha$	α^2
	2-D diffusion	D2	$[-\ln(1-\alpha)]^{-1}$	$\alpha+(1-\alpha)\ln(1-\alpha)$
	3-D diffusion-Jander	D3	$[(3/2)(1-\alpha)^{2/3}]/ [1-(1-\alpha)^{1/3}]$	$[1-(1-\alpha)^{1/3}]^2$
	Ginstling-Brounshtein	D4	$[(3/2)(1-\alpha)^{1/3}]/ [1-(1-\alpha)^{1/3}]$	$(1-2\alpha/3)- (1-\alpha)^{2/3}$
Nucleation	Avrami-Erofeyev	A2	$2(1-\alpha)[-\ln(1-\alpha)]^{1/2}$	$[-\ln(1-\alpha)]^{1/2}$
	Avrami-Erofeyev	A3	$3(1-\alpha)[-\ln(1-\alpha)]^{1/3}$	$[-\ln(1-\alpha)]^{1/3}$
	Avrami-Erofeyev	A1.5	$1.5(1-\alpha)[-\ln(1-\alpha)]^{1/3}$	$[-\ln(1-\alpha)]^{2/3}$
	Avrami-Erofeyev	A4	$4(1-\alpha)[-\ln(1-\alpha)]^{3/4}$	$[-\ln(1-\alpha)]^{1/4}$
Geometrical contraction	Contracting area	G2	$2(1-\alpha)^{1/2}$	$1-(1-\alpha)^{1/2}$
	Contracting volume	G3	$3(1-\alpha)^{1/3}$	$1-(1-\alpha)^{1/3}$
Power law	2/3-Power law	P2/3	$2/3\alpha^{-1/2}$	$\alpha^{3/2}$
	2-Power law	P2	$2\alpha^{1/2}$	$\alpha^{1/2}$
	3-Power law	P3	$3\alpha^{2/3}$	$\alpha^{1/3}$
	4-Power law	P4	$4\alpha^{3/4}$	$\alpha^{1/4}$

Table S6. Main compounds identified in liquid products at different conditions

Number	Residence time (min)	Compounds	GCMS/(area)%		
			80kg/h	50kg/h	30kg/h
1	2.351	Formic acid	2.38	2.14	1.94
2	2.597	Methyl formate	2.34	2.37	2.01
3	3.303	Acetic acid	26.24	24.89	22.65
4	3.475	2-Propanone, 1-hydroxy-	6.06	5.44	5.15
5	5.187	1-Hydroxy-2-butanone	1.95	2.00	1.84
6	6.567	Furfural	3.40	3.28	3.14
7	7.573	2-Furanmethanol	4.57	4.32	5.37
8	7.941	2-Propanone, 1-(acetyloxy)-	1.15	-	1.06
9	9.286	Butyrolactone	1.61	1.58	1.59
10	9.675	1,2-Cyclopentanedione	1.87	2.12	1.54
11	11.466	Phenol	3.21	3.44	4.04
12	12.945	2-Cyclopenten-1-one, 2-hydroxy-	2.52	2.43	2.16
13	14.364	P-Cresol	3.34	3.1	3.74
14	14.733	Phenol, 2-methoxy-	3.55	3.85	3.47
15	17.86	Creosol	6.23	6.08	6.39
16	18.215	Catechol	3.93	4.43	4.63
17	19.866	1,2-Benzenediol, 3-methoxy-	2.35	2.27	2.08
18	20.257	Phenol,4-ethyl-2-Methoxy-	1.46	1.59	2.32
19	22.281	Phenol, 2,6-dimethoxy-	1.95	1.44	2.47

Table S7. Compositions of liquid, gas products and element analysis of biochar at different conditions

Item	compound	30kg/h	50kg/h	80kg/h
1	Acids (area%)	24.59	27.03	28.62
2	Furans (area%)	8.51	7.6	7.97
3	Esters (area%)	1.59	1.58	1.61
4	Ketones (area%)	11.75	11.99	13.55
5	Phenols (area%)	30.14	26.2	23.02
6	H_2 (vol.%)	8.6	7.9	7.8
7	CO (vol.%)	39.1	32.6	23.9
8	CH_4(vol.%)	4.8	3.2	1.6
9	CO_2(vol.%)	47.5	56.3	66.7
10	C (wt.%)	47.513	46.726	46.153
11	H (wt.%)	3.037	2.527	2.492
12	N (wt.%)	0.92	0.866	0.863
13	S (wt.%)	0.02	0.018	0.01

Table S8. Parameters of techno-economic analysis for MAP (capacity: 50 kg/h)

Parameters	Value	Unit
Operation time	7500	hours/year
Temperature	260-280	^{o}C
Pressure	-20	kPa
Investment cost	42,253	$
Raw material intake	375	t/year
Bio-char output	186.8	t/year
Bio-oil output	110.6	t/year
Bio-gas output	77.6	t/year
Total equipment cos	112,676	$
Life of equipment	10	year
Equipment residuals rate	12.5%	
Material price	14.1	$/t
Maintenance	10.2	$/t
Electricity	21.1	$/t
Labor	28.2	$/t
Transportation	15.8	$/t

Techno-economic viability of large-scale microwave-assisted pyrolysis was evaluated based on the process that was tested in this study. The annual production scale was set for 375 ton biomass (rice straw). The price of bio-oil was X=1000 RMB/t, the price of biochar was Z=1617.5 RMB/t, the subsidy of biomass was B=150 RMB/ton, and the price of biogas was Y=231.9 RMB/t. The reaction temperature affected the capacity, electricity cost and product distribution, and it was set as 260^{o}C in the calculation. The price of raw material rice straw was 100 RMB/t (F), and the transportation fee within 10km was 112 RMB/t, including the cost of storage, unloading and loading of machinery, transportation, etc. The electricity cost was E=149.7 RMB/t, the operation cost was about M=272.7 RMB/t, consisting of direct wages, manufacturing costs, maintenance, bonuses, etc., The equipment costs was about 800,000 RMB, and residual value 100,000 RMB after 10 years. The annual depreciation was 70,000 RMB, the discount rate was i=8%, and the tax rate was 20%. The first phase advances operating capital was 300,000 RMB, which will be recovered after the project is completed. Thus, the primary cost of labor and electricity accounted for 30.3% and 22.7%, while the transportation and feedstocks cost were 16.9% and 15.2%, respectively.

$$NPV=\sum NCF*(1/(1+i)^{n})+(NCF+100000+300000)*(1/(1+i)^{10})-(300000+800000)$$

$$=\sum\{[(S+L+G+B)-A*(E+F+M+70000)]*(1-20\%)+70000\}*(1/(1+i)^{n})+\{[(S+L+G+B)-A*(E+F+M+70000)]*(1-20\%)+70000+100000+300000\}*(1/(1+i)^{10})-1100000$$

The sensitivity analysis of operation parameters was obtained based on the net present value (NPV), when it changed with the variation (15%) of a single parameter. the parameter changes in y-axis were

corresponding to the changes of the NPV in x-axis. Based on the best conditions, the bio-oil prices, biochar prices, biogas prices, transportation distances, operating expenses, capacity, temperature, electricity prices and return on investment were used as variables of sensitivity analysis. The steeper the parameters demonstrated the more effect on the NPV. The increases in return on capacity，bio-oil prices, biochar prices and biogas prices resulted in the increase in NPV. On the contrary, the discount rate，electricity, management，transportation price and temperature were relatively insignificant. Higher the temperature led to lower the biochar yield, which affected the NPV. The transportation distance showed a negative effect on NPV. Management costs included direct wages, manufacturing costs, packaging and transportation, maintenance, and other expenses such as bonuses. When the NPV >0, the project was economically acceptable. Therefore, the price of biochar cannot be lower than 3-5% of the original price, and the temperature cannot be higher than 5-8% of the baseline.

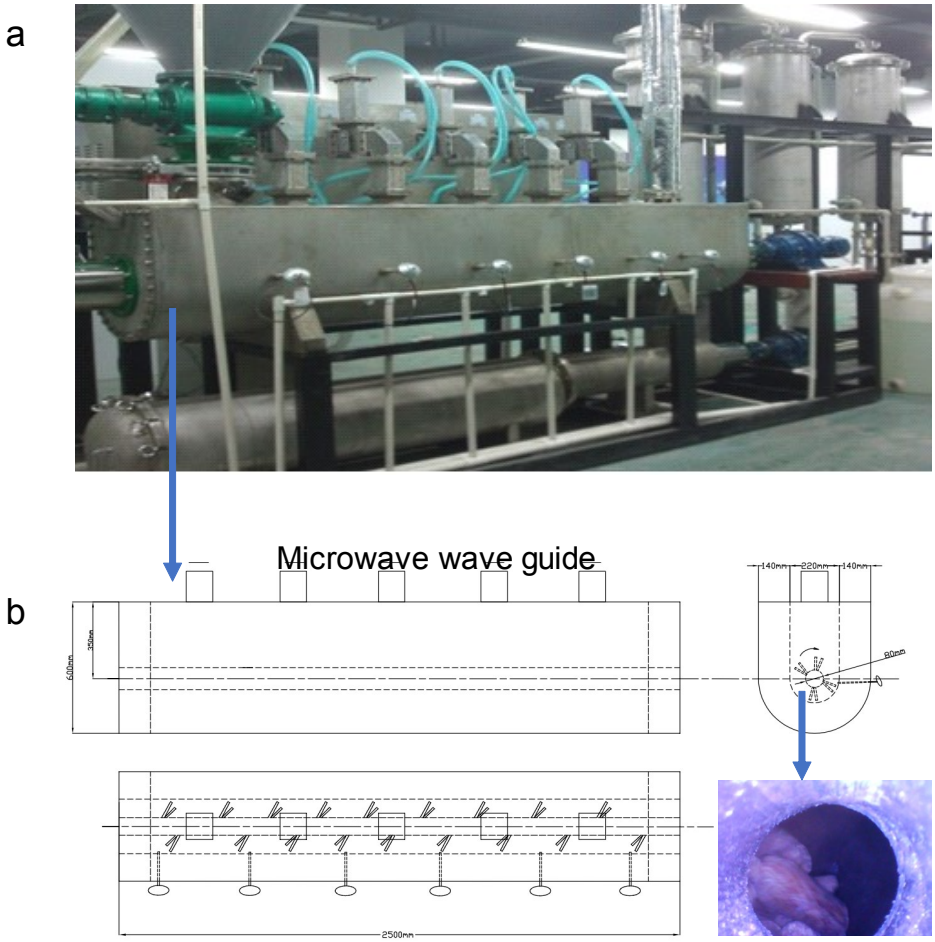

Fig. S1 a) Microwave-assisted auger reactor and b) structure and size of the main reactor

The pyrolysis system was consisted of a feeding hopper, microwave-assisted auger reactor, storage containers, condensers and filters. The conical shaped hopper (400 L) was installed on the upside of the rector, including a lock at the bottom with motor to maintain the feed rate from 0 to 80 kg/h. The singe auger reactor consisted of a 200 cm long and 220 mm diameter tube, and the screw rotation speed can be modified between 0 and 80 rpm with a speed variator. Five microwave waveguides were connected to the auger reactor with a total power of 15 kW, which can be adjusted with the programmed temperature. The temperatures of the materials were monitored by six thermocouples on the wall of the reactor. A char collector was located below the auger reactor with a reversed screw, and three condensers were applied to separate the liquid and gaseous products, where most of the bio-oil were condensed and collected in the first oil container. Circulating water with pumps was applied to cool down the microwave waveguide and the condensers. Two filters were used to absorb and separate the tar composition from gas, and the pyrolysis system was kept at a slight negative pressure (-20kpa) using a roots blower.

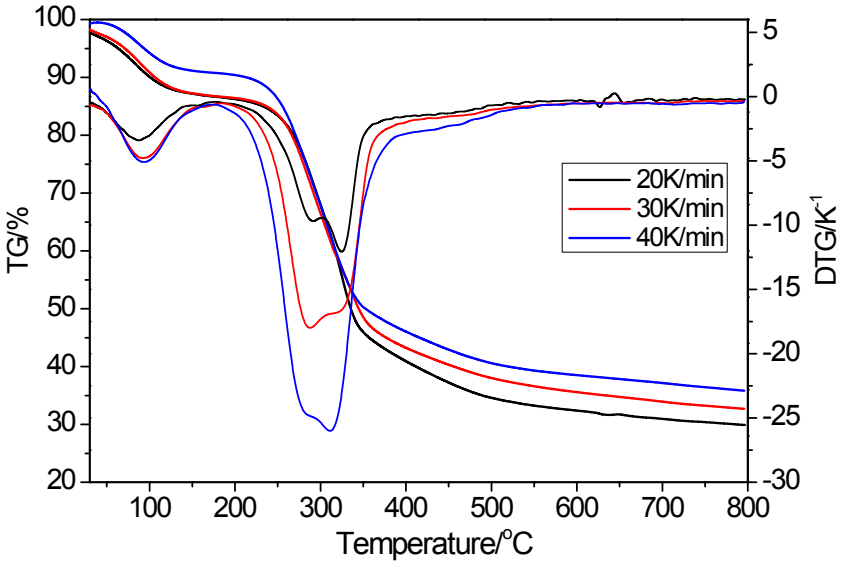

Fig. S2 TG/DTG curves for rice straw with conventional heating

Text S1: Detailed simulation process of MAP

The COMSOL Multiphysics 5.0 were applied to compute the numerical work of coupled electromagnetic and heat transfer equations for the MAP of rice straw using a finite element method (FEM). The microwave frequency was 2450 MHz and the heating mode of the reactor was TE_{10}. The length, width and height dimensions of the resonator were 420 mm × 320 mm × 320 mm, and the waveguide model was BJ-22. The diameter of the quartz reaction bottle was 2.6 cm, and the height was 12 cm.

The Maxwell equation can be used to simulate the electromagnetic field and describe the electromagnetic field distribution in the microwave cavity. The governing equation of the electric field wave is given by [17]:

$$\nabla \times \mu_r^{-1}(\nabla \times E) - k_0^2\left(\varepsilon_r - \frac{j\sigma}{\omega\varepsilon_0}\right)E = 0$$

where ω is the angular frequency, ε_r is the relative permittivity, σ is the conductivity rate, ε_0 is the dielectric constant of the vacuum (8.85×10^{-12} F/m)), μ_r is the relative permeability, k_0 is the wave number in free space and it is given by the expression (c_0 is the speed of light in vacuum):

$$k_0 = \omega\sqrt{\varepsilon_0\mu_0} = \frac{\omega}{c_0}$$

The dielectric properties were expressed as complex real and imaginary parts (ε' is the real dielectric constant, ε'' is the imaginary dielectric constant) by:

$$\varepsilon = \varepsilon' - j\varepsilon''$$

The heat transfer equation in the microwave field can use the Fourier energy balance equation by (Where ρ is the density (kg/m^3), k is the thermal conductivity of the material ($W/m^2/K$), Q is the heat source, C_p is the specific heat capacity (J/kg/K), and T is the temperature (K)):

$$\rho C_p\frac{\partial T}{\partial t} + \rho C_p u \cdot \nabla T = Q + \nabla \cdot (k\nabla T)$$

The magnetic conductor boundary conditions are used to define symmetric boundaries:

$$n \times H = 0$$

The adiabatic boundary condition is given by equation:

$$-n \times (-k\nabla T) = 0$$

The initial temperature conditions are: t=0, $T=T_0$=26.9 °C.

The grid is used to divide the microwave resonant cavity, and the optimization of the grid determines the calculation amount and calculation accuracy. The maximum grid in the microwave cavity is 20mm and

the minimum grid is 0.86mm. For the division network of the quartz reactor, the maximum grid size is 1.8mm and the minimum is 0.86mm. By calculating the coupling model of the electromagnetic field and the temperature field in the microwave cavity and the quartz reactor, the various field distributions in the wood chip reaction process can be obtained.

Text S2: Detailed calculation of pyrolysis kinetics

The conversion rate α of the sample in the experiment is identified by Eq.(1), where m_0 and m_e are the initial and final mass of the sample, respectively; m_t is the mass of sample at a given time.

$$\alpha = \frac{m_0 - m_t}{m_0 - m_e} \quad (1)$$

Under the linear heating rate ($\beta = dT/dt$), the apparent reaction rate of biomass components pyrolysis according to Arrhenius law is expressed as [18] Eq. (2), where A is the pre-exponential factor; E is the activation energy; R is the universal gas constant; t is the duration time of reaction; T is absolute temperature.

$$\frac{d\alpha}{dT} = \frac{A}{\beta} exp\left(\frac{-E}{RT}\right) f(\alpha) \quad (2)$$

For single reaction, isoconversional methods are deemed to accurately estimate the apparent activation energy without assuming any form of mechanism function $f(\alpha)$. As recommended by the ICTAC Kinetics Committee,[19] Kissinger-Akahira-Sunose (KAS) equation is accurate to estimate E_α by using multiple heating rates:

$$\ln\left(\frac{\beta}{T_\alpha^{1.92}}\right) = Const - 1.008\left(\frac{E_\alpha}{RT_\alpha}\right) \quad (3)$$

where E_α and T_α are the activation energy and temperature at given α, respectively. For constant α, E_α can be determined by the slope of the straight line by plotting $\ln(\beta/T_\alpha^{1.92})$ vs. $1/T_\alpha$. Through KAS method, we can get different activation energy values during the pyrolysis process depending on the conversion degree.

The kinetic model $f(\alpha)$ is an algebraic expression associated with the physical model of the reaction. In this work, the $y(\alpha)$ master-plots method was used to determine the most appropriate kinetic model of biomass components pyrolysis. The $y(\alpha)$ function could be defined as the following forms:[20]

$$y(\alpha) = \left(\frac{d\alpha}{dt}\right)_\alpha \exp\left(\frac{E_0}{RT_\alpha}\right) = Af(\alpha) \quad (4)$$

where E_0 is the average value of E_α calculated from KAS method; $(d\alpha/dt)_\alpha$ is the differential conversion vs. differential time at given α and heating rate. The experimental $y(\alpha)$ plots can be obtained by plotting $y(\alpha)$ vs. α, and the theoretical $y(\alpha)$ plots can be also obtain by plotting $f(\alpha)$ vs. α with the same α. However, as the unknown of pre-exponential factor (A), the experimental and theoretical $y(\alpha)$ plots should be normalized to 0-1 range in a same way. The following equation is used to normalize the experimental and theoretical $y(\alpha)$.[18, 21] The suitable mechanism models of biomass components are obtained by comparing

the experimental and theoretical $y(\alpha)_{norm}$.

$$y(\alpha)_{norm} = \frac{y(\alpha)}{max[y(\alpha)]} \quad (5)$$

After E_α and the reaction model $f(\alpha)$ have been identified, the A_α can be obtained by using energy compensation effects.[22] The relationship of A_α and E_α is known as：

$$lnA_\alpha = aE_\alpha + b \quad (6)$$

$$lnA_0 = aE_0 + b \quad (7)$$

where a and b are constants. The plot of $\ln A_\alpha$ vs. E_α will give a straight line and a, b can be estimated from the slope and intercept, respectively. And then the mean value of pre-exponential factor (A_0) can be estimated by Eq. (7).

Text S3: Net energy ratio calculation

The net energy ratio (NER) was defined by the equation: NER= Ei/Eo. [23, 24]

Where Ei was the total energy input, and it contained the embodied energy of materials (E1) and the electricity consumption for the machinery (E2). E1 was calculated by the equation: E1=HHV×m. The HHV is higher heating value and m is the mass of the raw material. E2 is obtained from the actual consumption shown by the power meter.

Eo was the total energy output, and it contained the embodied energy of products (E3) and the specific enthalpy (E3). E3 was calculated by the equation: E3=HHV×m. The HHV is higher heating value and m is the mass of the different products. E4 is obtained from the equation, E4= (m1×C1+ m2×C2+ m3×C3) ×(T1- T2). Where m1, m2 and m3 represented the mass of bio-char, bio-oil and bio-gas, C1, C2 and C3 represented the heat capacity of bio-char, bio-oil and bio-gas, T1 and T2 are the final and initial temperature of the reaction.

Text S4: Experiment procedures

Rice straw used in the experiment was derived from Chongming District, Shanghai, China. It was naturally dried and the main characteristics were listed in Table S6. The proximate analysis was carried out according to the ASTM standards, [21, 25] and the elemental analysis was tested by the Thermo Scientific Flash 2000 analyzer with a dry basis. Rice straw was sieved to 10-20 mesh for bench experiment, and it was pelleted with diameter of 5 mm and length of 25mm for the pilot test. All solvents were purchased from Sinopharm Chemical Reagent Co., (Shanghai, China).

Table S9. Characteristics of rice straw

Proximate analysis (wet basis, wt.%)		Elemental analysis (dry basis, wt.%)	
Moisture content	10.36	C	34.97
Ash content	15.80	H	4.99
Volatiles	67.30	N	0.68
Fixed carbon	6.54	O[a]	59.36

[a] Calculated by difference.

The MAP of rice straw was carried out using a microwave heating system (XTrust Analytical Instruments Co., Ltd, Shanghai, China), as shown in Fig.S3. It mainly consisted of a microwave oven, a quartz tube reactor and connected condensers, and the detailed information was described in our precious work. [25] After connecting the inlet and outlet quartz tubes, the oven was heated to designed temperature, and then rice straw dropped into the reactor. After reaction, the volatiles were captured by condensers, and the yield of solid and liquid products were calculated from their weight, while the gas yield was obtained by differences based on the mass balance. In all cases, the average values were calculated through three repeated trials.

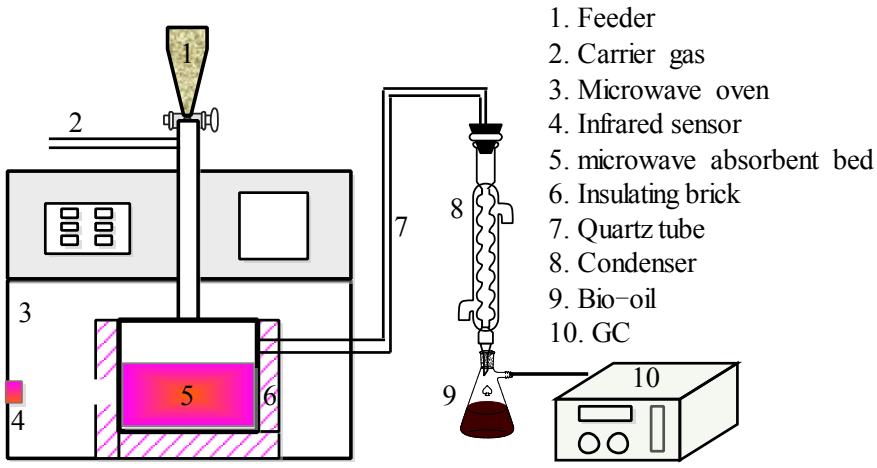

Fig. S3 The schematic diagram of the microwave-assisted pyrolysis reactor

Microwave thermogravimetric analysis (MW-TGA) of rice straw was conducted in a MW-TGA apparatus, as shown in Fig. S4 and the detailed information was described in precious work [25-27]. The sample was heated by a microwave oven with a maximum power of 1300 W, and the temperature profiles of the reactor were measured and controlled by an infrared thermometer. The infrared thermometer (-25~900 °C) was located in the middle of the back side and just below the PTFE window, which was calibrated with thermocouples in the samples during the cooling process (from 900~30 °C) after the MW was turned off. The flow rate of N_2 was 300 mL/min to keep an oxygen-free environment during the reaction. The rice straw sample was heated from 25 °C to 550 °C with three heating rates of 20, 30 and 40K/min. Temperature and weight variation were automatically recorded during the experiments. In all cases, the average values were obtained through three repeated trials.

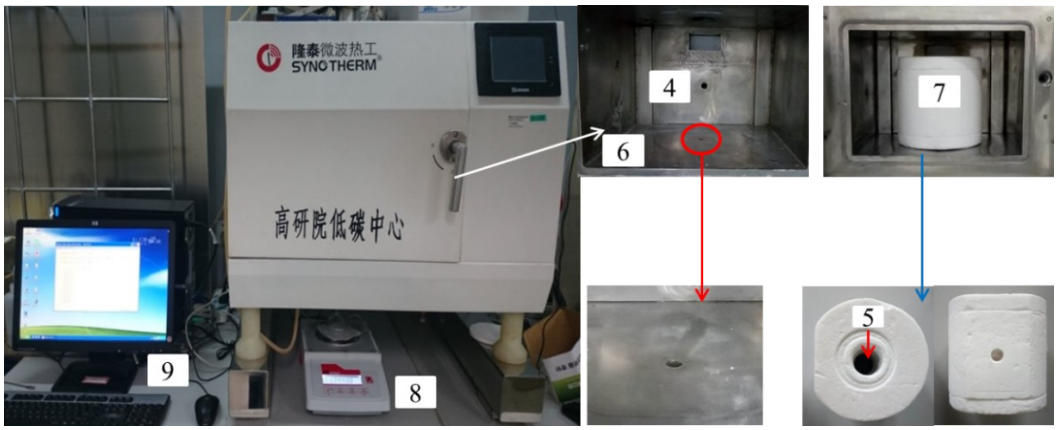

Fig. S4. The schematic diagram of MW-TGA apparatus.

1-Carrier gas, 2-Mass flow control, 3-Quartz tube, 4-Infrared sensor, 5-Sample, 6-Microwave Oven, 7-Insulating Brick, 8-Electronic Balance, 9-Computer

Text S5: Products Analysis

The liquid products were analyzed by an Agilent 7890-5975C gas chromatography-mass spectrometer with an HP-5 MS capillary column. The flow rate of carrier gas Helium (99.999%) was kept at 1 mL/min. The temperature in the injector and ion source was maintained at 250 ^{o}C and 230 ^{o}C. The oven was kept at 60 ^{o}C for 3 min and increased to 280 ^{o}C with a heating rate of 5 ^{o}C /min, and then it was held for 10 min. The analysis and identification of liquid components were performed with the National Institute of Standards and Technology (NIST) mass spectral data library.[25, 28] Elemental analysis of solid products was tested by the Thermo Scientific Flash 2000 analyzer with a dry basis. Varian Micro-GC with a thermal conductivity detector (TCD) was used to analyze the gaseous product after reaction. Channel A was operated at 95 ^{o}C to analyze the content of H_2, CO and CH_4 with a molecular sieve 5A column, and channel B was kept at 60 ^{o}C to determine the content of CO_2 with a Porapak Q (PPQ) column.[27, 28] The metal elemental concentrations were obtained by the inductive coupled plasma (ICP) ion spectrometry (Perkin Elmer Optima 3000).

References

1 J. Park, Y. Lee, C. Ryu and Y. K. Park, *Bioresour Technol*, 2014, **155**, 63-70.

2 B. Biswas, R. Singh, J. Kumar, R. Singh, P. Gupta, B. B. Krishna and T. Bhaskar, *Renew Energ*, 2018, **129**, 686-694.

3 S.-H. Jung, B.-S. Kang and J.-S. Kim, *J Anal Appl Pyrol*, 2008, **82**, 240-247.

4 H. Nam, S. C. Capareda, N. Ashwath and J. Kongkasawan, *Energy*, 2015, **93**, 2384-2394.

5 S. Ukaew, J. Schoenborn, B. Klemetsrud and D. R. Shonnard, *J Anal Appl Pyrol*, 2018, **129**, 112-122.

6 A. M. Shoaib, R. A. El-Adly, M. H. M. Hassanean, A. Youssry and A. A. Bhran, *Egyptian Journal of Petroleum*, 2018, **27**, 1305-1311.

7 X. Jin, N. Chen-yang, Z. Deng-yin, G. Yan-hui, H. Qi-min, X. Yu-hong and B. paul, *Biomass Bioenergy*, 2019, **127**, 105281.

8 Y. F. Huang, P. T. Chiueh, W. H. Kuan and S. L. Lo, *Bioresour Technol*, 2013, **142**, 620-624.

9 C. Ravikumar, P. Senthil Kumar, S. K. Subhashni, P. V. Tejaswini and V. Varshini, *Sustainable Materials and Technologies*, 2017, **11**, 19-27.

10 L. F. Calvo, M. Otero, B. M. Jenkins, A. Morán and A. I. Garćıa, *Fuel Process Technol*, 2004, **85**, 279-291.

11 G. Jiang, D. J. Nowakowski and A. V. Bridgwater, *Thermochim. Acta*, 2010, **498**, 61-66.

12 G. Mishra and T. Bhaskar, *Bioresour Technol*, 2014, **169**, 614-621.

13 D. Chen, Y. Wang, Y. Liu, K. Cen, X. Cao, Z. Ma and Y. Li, *Fuel*, 2019, **252**, 1-9.

14 Y. Huang, P. Chiueh, W. Kuan and S. Lo, *Energy*, 2016, **100**, 137-144.

15 J. Liang, H. M. Morgan, Y. Liu, A. Shi, H. Lei, H. Mao and Q. Bu, *J Anal Appl Pyrol*, 2017, **128**, 324-334.

16 H.-S. Tai and C.-Y. Chen, *Environ Eng Sci*, 2016, **33**, 671-680.

17 Y. D. Hong, B. Q. Lin, H. Li, H. M. Dai, C. J. Zhu and H. Yao, *Appl. Therm. Eng.*, 2016, **93**, 1145-1154.

18 S. Vyazovkin, A. K. Burnham, J. M. Criado, L. A. Perez-Maqueda, C. Popescu and N. Sbirrazzuoli, *Thermochim. Acta*, 2011, **520**, 1-19.

19 S. Vyazovkin, K. Chrissafis, M. L. Di Lorenzo, N. Koga, M. Pijolat, B. Roduit, N. Sbirrazzuoli and J. J. Sunol, *Thermochim. Acta*, 2014, **590**, 1-23.

20 X. Wang, M. Hu, W. Hu, Z. Chen, S. Liu, Z. Hu and B. Xiao, *Bioresour. Technol.*, 2016, **219**, 510-520.

21 M. Hu, Z. Chen, D. Guo, C. Liu, B. Xiao, Z. Hu and S. Liu, *Bioresour Technol*, 2015, **177**, 41-50.

22 M. Hu, Z. Chen, S. Wang, D. Guo, C. Ma, Y. Zhou, J. Chen, M. Laghari, S. Fazal, B. Xiao, B. Zhang and S. Ma, *Energy Convers. Manage.*, 2016, **118**, 1-11.

23 E. G. Nwoba, D. A. Parlevliet, D. W. Laird, K. Alameh, J. Louveau, J. Pruvost and N. R. Moheimani, *Appl Energ*, 2020, **275**, 115403.

24 F. Naaz, A. Bhattacharya, K. K. Pant and A. Malik, *Appl Energ*, 2019, **254**, 113656.

25 H. Luo, L. Bao, L. Kong and Y. Sun, *Bioresour Technol*, 2017, **238**, 109-115.

26 H. Luo, L. W. Bao, L. Z. Kong and Y. H. Sun, *AlChE J*, 2018, **64**, 2124-2134.
27 H. Luo, H. Wang, L. Kong, S. Li and Y. Sun, *J Hazard Mater*, 2019, **377**, 341-348.
28 H. Luo, L. Bao, H. Wang, L. Kong and Y. Sun, *Bioresour Technol*, 2018, **267**, 333-340.